ACS APPLIED ENERGY MATERIALS

www.acsaem.org Article

Perfluoroarene-Based 2D/3D Perovskite Solar Cells

Published as part of ACS Applied Energy Materials special issue "Global Conference for Decarbonization of Energy and Materials 2023".

Weifan Luo,[⊥] Jong-Min Kim,[⊥] Paul Zimmermann, Tim Hügli, Sun-Ju Kim, Mengqiong Zhu, Ghewa AlSabeh, Alexander Hinderhofer, Frank Schreiber, Jovana V. Milić,* and Ji-Youn Seo*

Cite This: *ACS Appl. Energy Mater.* 2025, 8, 8914–8920 Read Online

ACCESS | Metrics & More | Article Recommendations | Supporting Information

ABSTRACT: Hybrid organic−inorganic layered (2D) halide perovskites have demonstrated advantages in improving the performance and stability of perovskite solar cells, and there is an ongoing interest in tailoring organic cations for their application in photovoltaics. We apply tailored molecular systems based on perfluorinated benzylammonium (F-BNA) and 1,4-phenylenedimethylammonium (F-PDMA) cations, forming Ruddlesden−Popper and Dion−Jacobson perovskite phases, respectively, at the interface with 3D perovskite layers in conventional n−i−p perovskite solar cells. The characteristics of 2D/3D perovskite phases are investigated through a combination of techniques including X-ray diffraction, UV−vis absorption, and photoluminescence spectroscopy. We demonstrate the beneficial effects of perfluoroarene perovskite phases in improving the stability and performance toward advancing photovoltaics.

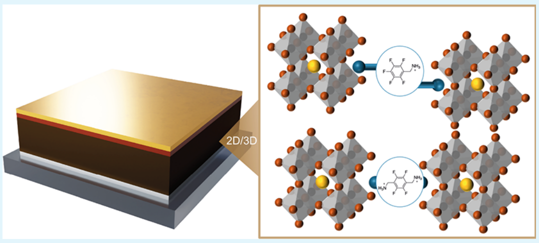

KEYWORDS: *mixed-dimensional perovskites, 2D/3D perovskites, perfluoroarenes, interfacial engineering, photovoltaics*

■ INTRODUCTION

In recent years, there has been a growing interest in exploring 2D/3D perovskite structures, aiming to merge the favorable attributes of 2D and 3D perovskite materials.[1,2] This hybrid approach seeks to capitalize on the stability inherent in 2D perovskites while harnessing the high efficiency associated with their 3D counterparts.[1] Metal halide perovskites are described by the general formula AMX_3 (Figure 1), where A denotes the central cation (e.g., methylammonium MA^+, formamidinium FA^+, or Cs^+), M represents a divalent metal ion (predominantly Pb^{2+} or Sn^{2+}), and X signifies a halide anion (I^-, Br^-, or Cl^-).[3] Their layered (2D) perovskite analogues have gained considerable interest due to their superior stability compared with 3D perovskite materials.[4] They are formed by introducing spacer cations between the layers of hybrid perovskites (Figure 1),[4] leading to the formation of common Ruddlesden−Popper (RP) and Dion−Jacobson (DJ) phases.[5] RP systems typically have the general formula $S_2'A_{n-1}M_nX_{3n+1}$, where S′ denotes monofunctional spacers, resulting in the formation of a bilayer structure with a half-unit-cell displacement between adjacent layers (Figure 1). Conversely, DJ systems are characterized by the formula $SA_{n-1}M_nX_{3n+1}$, incorporating bifunctional spacer (S) moieties between aligned perovskite layers.[6−9] Spacer cations can tune the properties of 2D perovskites, their morphology, and structure, forming a natural quantum-well electronic structure and altering the band gap while serving as protective layers that increase hydrophobicity and prevent ion migration.[4,10] There is a significant interest in incorporating these materials into perovskites due to their structural diversity

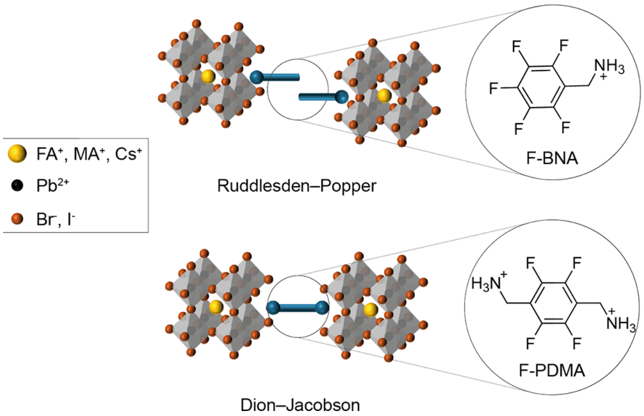

Figure 1. Layered hybrid perovskite structure. Schematic of the layered (2D) perovskite structure with the Ruddlesden–Popper (RP) and Dion–Jacobson (DJ) perovskite phase (represented by $n = 2$ compositions) and structures of F-BNA and F-PDMA perfluoroarenes.

Received: July 11, 2024
Revised: May 22, 2025
Accepted: May 26, 2025
Published: June 24, 2025

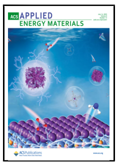

https://doi.org/10.1021/acsaem.4c01710
ACS Appl. Energy Mater. 2025, 8, 8914–8920

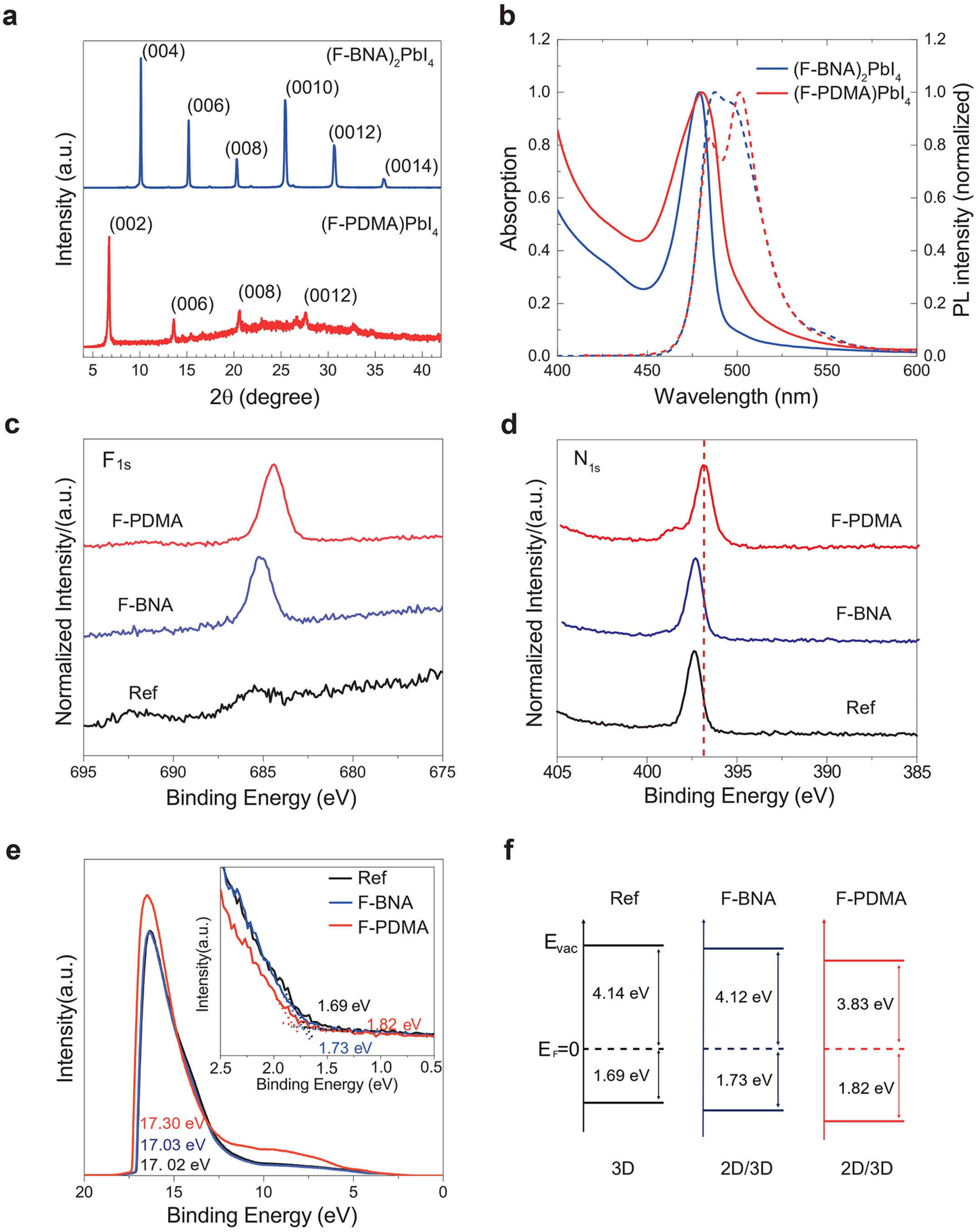

Figure 2. Structural and optoelectronic properties of 2D and 2D/3D perovskites. (a) XRD pattern and (b) UV−vis absorption and PL spectra of the perfluoroarene-based 2D perovskite films of $n = 1$ nominal composition. (c,d) XPS F 1s and N 1s core level spectra of the 3D control (ref, black) and 2D/3D perovskite films with either F-BNA (blue) or F-PDMA (red) overlayers. (e) UPS spectra of the control (ref) and treated (F-BNA or F-PDMA) perovskite films, with the secondary electron cutoff (SECO) for determining the work function. The binding energy of the valence band spectra is shown in the inset, and the kinetic energy is in Figure S19 of the Supporting Information. (f) Energy level diagram estimate.

and stabilizing potential.[11] In particular, the use of mixed-dimensional 2D/3D perovskite heterostructures, with the capacity to simultaneously improve photovoltaic performances and stabilities through a synergy of 2D and 3D perovskite layers, has been relevant to advancing perovskite photovoltaics.[1,2] They are accessed by depositing 2D perovskites or organic spacer cations onto 3D perovskite layers.[1,2]

To this end, perfluorinated organic moieties are particularly noteworthy since introducing fluorine can enhance the hydrophobicity and suppress ion migration.[12,13] Accordingly, perfluoroarenes are of interest to tailoring structural and optoelectronic properties of 2D perovskites toward their applications.[13−15] The perfluoroarene systems are relevant to controlling hybrid perovskite assemblies through π-based interactions, hydrogen bonding, van der Waals forces, as well as halogen bonding.[4,11,13] These interactions can modify the optoelectronic and structural properties of the hybrid materials. For example, hydrogen bonding can regulate perovskite assemblies and the activation energy for ion migration.[13] Additionally, π−π interactions between arene and perfluoroarene species can create an alternating-cation 2D perovskite system through self-assembly.[16] This results in a more compact parallel stacking in arene−perfluoroarene systems, altering charge transport.[16−18] In this regard, the emerging 2D/3D perovskite heterostructures[1,2,19−21] provide a relevant platform for perfluoroarenes. However, these (supra)-molecular systems remain underexploited for their potential to tailor the properties of the interface with charge-selective extraction layers in mixed-dimensional perovskite photovoltaics.

Here, we applied perfluorinated benzylammonium (F-BNA) and 1,4-phenylenedimethylammonium (F-PDMA) iodides as uniquely tailored model systems that form RP and DJ 2D perovskite overlayers, respectively, onto 3D perovskites in the corresponding solar cells. The formation of 2D/3D heterostructures was investigated by a combination of techniques, including X-ray diffraction, X-ray photoelectron spectroscopy, UV−vis absorption, and photoluminescence spectroscopy. We integrated the 2D/3D perfluoroarene-based perovskite layers into n−i−p perovskite solar cells, achieving a power conversion efficiency (PCE) up to 20% for champion devices compared to 18% for a control device without the 2D/3D structure. Moreover, the devices displayed operational stability with 85% performance retention after 750 h, showcasing the relevance of perfluoroarene-based perovskites in photovoltaics.

■ RESULTS AND DISCUSSION

The perfluoroarene spacers were synthesized by reducing tetrafluoroterephthalonitrile or pentafluorobenzonitrile precursors, followed by protonation of the resulting amines in accordance with the previous reports,[16−18] as detailed in the Experimental Section of the Supporting Information (Figures S1−S6). The spacer precursors, F-BNAI or F-PDMAI$_2$, were thereafter used to prepare materials by reacting them with stoichiometric amounts of PbI$_2$ to obtain 2D perovskites of n = 1 nominal composition. This was achieved through solution processing (spin-coating) of films onto glass substrates, followed by annealing at 130 °C. The effectiveness of perfluoroarene-based 2D perovskites was thereafter analyzed in 2D/3D perovskite heterostructures by applying organic spacers from the solution of F-BNAI or F-PDMAI$_2$ (1 mg/mL concentration in isopropanol) onto conventional 3D (Cs$_{0.05}$FA$_{0.83}$MA$_{0.17}$)Pb(I$_{0.83}$Br$_{0.17}$)$_3$ compositions, forming 2D overlayers upon annealing in n−i−p perovskite solar cells.

The structural properties of hybrid materials were analyzed using X-ray diffraction (XRD). The low-angle reflections (2θ below 10°) accompanied by periodic reflections indicate the formation of a layered (2D) perovskite structure (Figure 2a).[22] For (F-BNA)$_2$PbI$_4$, a peak below 14° was identified, corresponding to the (004) reflection. A comparable result was obtained for the (F-PDMA)PbI$_4$ system. Moreover, grazing-incidence X-ray scattering (GIWAXS) measurements showed consistent results with an additional peak for (F-BNA)$_2$PbI$_4$ at 5° (0.35 Å^{-1}). Additionally, GIWAXS indicated that the long unit cell axis is preferentially oriented parallel to the substrate for (F-BNA)$_2$PbI$_4$ (Figure S7), whereas for (F-PDMA)PbI$_4$, it was mainly oriented parallel to the surface normal, with a substantial amount of randomly oriented n = 1 2D phases (Figure S8). For the F-BNA phase, we determined a unit cell consistent with the GIWAXS data (Figure S9). At room temperature, we found a tetragonal unit cell for (F-BNA)$_2$PbI$_4$ (n = 1) with the unit cell parameters $a = b$ = 8.55(8) Å, c = 35.6(4) and a volume of V = 2602(78) Å^3 (Table S1). The optoelectronic properties of 2D phases were further analyzed by UV−vis absorption and photoluminescence (PL) spectroscopy (Figure 2b). The excitonic features in the absorption spectra at around 460 nm corroborate the formation of 2D structures.[5,18,23] In addition, the PL spectra of F-PDMA-based films (Figure S10) exhibit multiple signals indicative of disorder, consistent with prior reports,[16] which require further investigation.

Having evidenced 2D perovskite formation, the structural properties of the 2D/3D perovskite materials were further analyzed. GIWAXS measurements were conducted to assess the effect of the spacers on the 3D perovskites, which showed no change in the orientation upon their use (Figure S11). All samples showed a preferred orientation of approximately 35° and 65° toward the substrate (Figure S12). Moreover, the control 3D sample was composed mainly of a cubic perovskite and some PbI$_2$ traces, whereas the F-PDMA-treated sample showed a peak at 0.5 Å^{-1}. The same peak was found for the pure (F-PDMA)PbI$_4$ phase, indicating the formation of a 2D (n = 1) layer on top of the 3D perovskite accompanied by the reduction of PbI$_2$ and hexagonal phase in the underlying 3D perovskite layer (Figure S13). Furthermore, X-ray photoelectron spectroscopy (XPS) measurements were performed on 3D and 2D/3D perovskite films to evaluate the formation of the overlayers (Figure 2c,d) by analyzing changes in the chemical environment. The untreated (control) 3D perovskite films exhibited no detectable fluorine (F) signal, whereas a distinct F 1s core level signal emerged at 685 eV for the 2D/3D perovskite films. In addition, the N 1s spectra of the 3D perovskite films featured characteristic C−N bonds (397.5 eV) associated with the A cation (Figure 2d, Table S2).[24] F-PDMA-treated samples exhibited a more pronounced (0.5 eV) shift toward lower binding energy compared with the control film. This indicates that the F-PDMA-based overlayer interacts more with the surface (e.g., Pb^{2+} or I$^-$), altering the electronic structure around nitrogen, which is more pronounced than the F-BNA systems. These interactions result in an increased electron density around the nitrogen atom, which was more pronounced compared to the C 1s XPS spectra (Figure S14), suggesting interactions predominantly taking place through the ammonium groups.[24] The effects of the interaction on the interfacial energetics were further analyzed using ultraviolet photoemission spectroscopy (UPS), with the bandgap estimated using PL spectra and the Tauc plots with the corresponding UV−vis absorption spectra. The work function (WF) showed differences of 0.02 and 0.26 eV between the reference and F-BNA- or F-PDMA-treated films, respectively (Figure 2e). Furthermore, the valence band (VB) maxima were 0.04 and 0.13 eV lower than the reference for treated films, respectively. UPS analysis confirmed that the energy level of the perovskite film changes when F-BNA or F-PDMA is applied, with the valence band (VB) tending to shift. While the energy alignment featured a minor mismatch at the hole transport layer (Figure 2f), the thickness of the overlayer did not compromise charge transport.[25,26] This was further analyzed by steady-state and time-resolved PL spectroscopy (TRPL). The PL spectra of 2D/3D perovskites revealed a reduced intensity upon applying the 2D overlayer, which can be related to an increase in nonradiative recombination due to changes in the interfacial defect concentration (Figure S15). This observation is consistent with the TRPL data of the perovskite films, showing longer charge-carrier lifetimes for reference 3D perovskite materials (Figure S16 and Table S3).

https://doi.org/10.1021/acsaem.4c01710
ACS Appl. Energy Mater. 2025, 8, 8914−8920

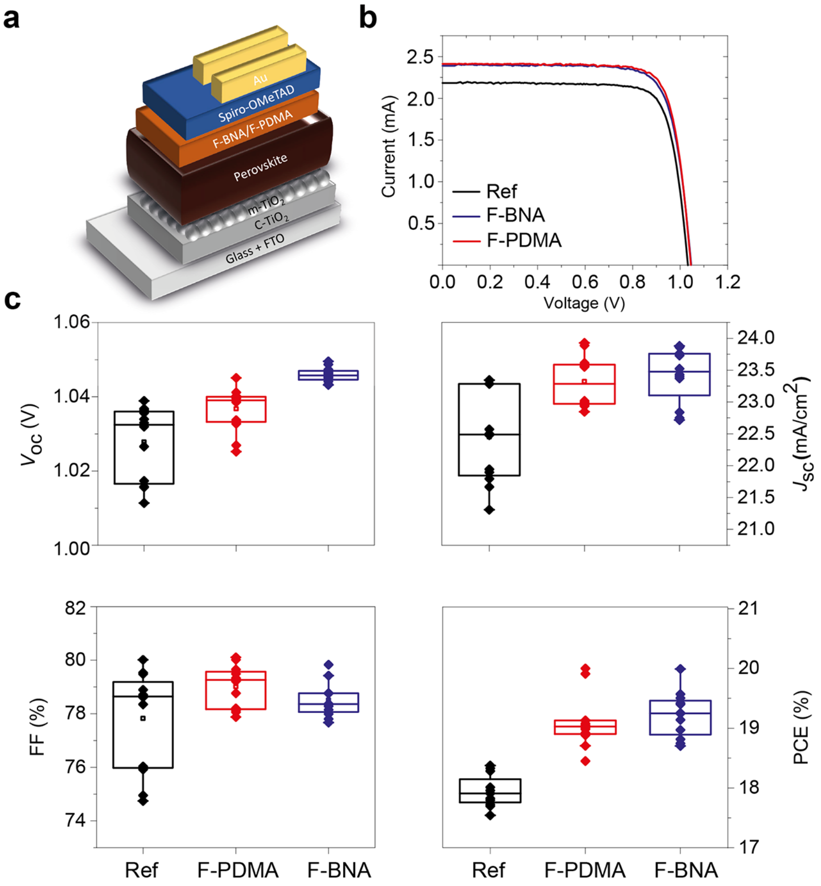

Figure 3. Photovoltaic performances in 2D/3D perovskite solar cells. (a) Schematic of the n−i−p solar cell. (b) *J*−*V* curves of the champion control, F-BNA-, and F-PDMA-treated devices under the AM 1.5G illumination. (c) Statistical distribution of the open-circuit voltage (V_{OC}), short-circuit current density (J_{SC}), fill factor (FF), and power conversion efficiency (PCE) for control, F-BNA-, and F-PDMA-treated (18) devices.

However, in the presence of the hole-transport layer, a faster decay was observed for the treated samples than in the control, suggesting that the perfluoroarene layers do not act as a barrier for charge extraction (Figure S17). By applying an exponential fit to the TRPL decays, the extraction time was estimated (Table S4), suggesting a facilitated charge extraction in the 2D/3D perovskite heterostructures to the 2,2′,7,7′-tetrakis-(*N*,*N*-di-4-methoxyphenylamino)-9,9′-spirobifluorene (Spiro-OMeTAD).[27] This is likely the result of arene−perfluoroarene interactions[16−18] with the hole-transporting material, which were envisaged to stabilize the interface with the hole-extraction layer and improve the contacts relevant to device performance and long-term stability. Furthermore, the analysis of the morphology of the 2D/3D structures by scanning electron microscopy (SEM) showed an increased grain size in the 2D/3D perovskite samples (Figure S18), which is further relevant to their charge extraction and the photovoltaic performance. The SEM images also reveal gaps that may result from solvent evaporation or the escape of volatile molecules from the surface. The passivation effect at grain boundaries can nonetheless minimize device performance losses, whereas further optimization of the morphology offers space for improving device performance in the future.

The performance of 2D/3D perovskites in photovoltaics was investigated in solar cells based on the n−i−p architecture of fluorine-doped tin oxide (FTO)/c-TiO$_2$/mp-TiO$_2$/perovskite/Spiro-OMeTAD/Au (Figure 3a). Their performance was evaluated by measuring the current−voltage (*J*−*V*) characteristics with a AM 1.5G light source (Figure 3b). The use of 2D/3D perovskite heterostructures with spacer overlayers resulted in increased open-circuit voltage (V_{OC}) and short-circuit current density (J_{SC}) while maintaining an unchanged fill factor (FF), thereby enhancing the overall PCE (Figure 3c). The increase in the V_{OC} was in accordance with the passivation effect at the interface, consistent with TRPL and SEM measurements, whereas a slightly reduced bandgap (estimated to be 1.59 eV for the control and 1.55 eV for the 2D/3D perovskites) was reflected in the improvements of the J_{SC}, leading to the overall improved performances. The *J*−*V* curves of the devices also exhibited a small hysteresis (Figure S20). The champion devices yielded PCEs of 18.4%, 20.0%, and 20.0% for the 3D, F-BNA-, and F-PDMA-treated samples, respectively (Table S5).

To further optimize the device performance, MACl was incorporated either by using 10 mol % into the perovskite precursor solution as an additive or by applying an overlayer (o.l.; 3 mg/mL in isopropanol) onto the reference 3D perovskite (Figures S21−S24).[28−30] This strategy led to an increase in V_{OC} and a slight improvement in FF, leading to an overall increase in PCE (up to 1.5%) upon treatment. Conversely, applying 2D overlayers onto these films resulted in a slight reduction in J_{SC} and FF, while V_{OC} remained comparable (Figure S25). The overall PCE remained similar, indicating that 2D overlayers did not significantly impact the MACl-treated films. The *J*−*V* curves of the champion devices showed a more significant hysteresis (Figure S26), with higher

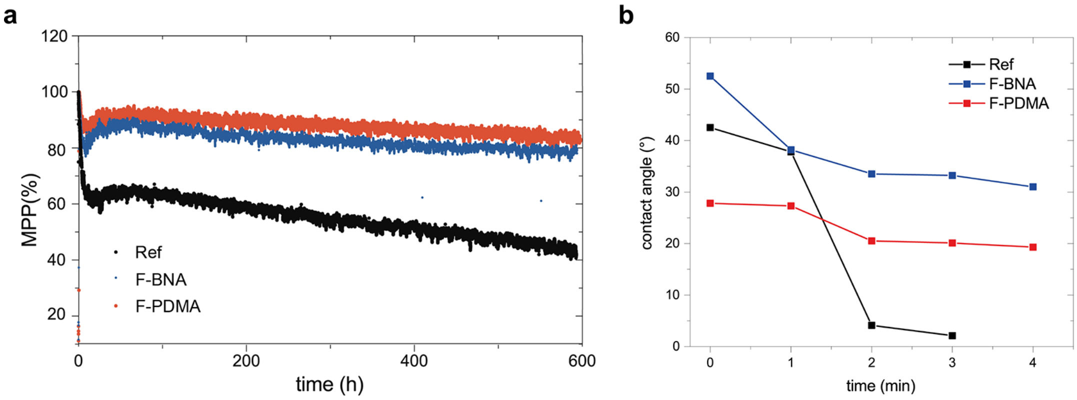

Figure 4. Operational stability in 2D/3D perovskite solar cells. (a) The evolution of the PCE during operation by MPP tracking optimized control, F-BNA-, and F-PDMA-treated solar cells (with MACl added to the 3D perovskite) in a nitrogen atmosphere under 1 sun irradiation at ambient temperature. (b) Contact angle measurement of a water droplet on the surface over time of 3D perovskite films (ref) and 3D/2D films with the F-PDMAI$_2$ (red) or F-BNAI (blue) overlayer.

PCEs observed for champion devices of 19.9% for the 3D control, 20.2% for the MACl-based additive, and 20.7% for the MACl overlayer, whereas 20.3% for the F-BNA and 20.5% for the F-PDMA-treated samples. While these performances can be further optimized, the analysis suggests that the treatment of the 3D perovskite with MACl has a more pronounced effect on photovoltaic performance, whereas the 2D overlayer is expected to influence stability.

The operational stability was assessed by monitoring the evolution of the maximum power point (MPP) of n−i−p devices (2−4 devices per condition to ensure reliability) under continuous 1 sun irradiation in a nitrogen atmosphere at ambient temperature, comparing reference devices with and without MACl treatment, as well as upon the use of perfluoroarenes (Figures 4 and S28). The F-BNA- and F-PDMA-treated samples demonstrated a significant advantage over the 3D control devices, degrading only by around 20% after more than 500 h (Figures 4a, S27). We observed a faster decrease in MPP at the beginning, likely due to defects at the perovskite interface, causing the initial rapid drop in MPP, which may undergo self-healing after a certain time, improving surface defects and slowing down the rate of degradation.[31] In contrast, the reference devices with MACl showed more pronounced degradation, particularly without a 2D overlayer, with their power output decreasing by approximately 80% after 600 h (Figure S28). These improvements in operational stability can be associated with interactions at the interface and increased hydrophobicity upon treatment, as evidenced by contact angle measurements with a water droplet (Figures 4b and S28). The increase in the hydrophobicity is further relevant to the improvement in the contacts with the hole-transport layer, corroborating the structural and optoelectronic characteristics, which underscore the impact of perfluoroarenes in photovoltaics.

■ CONCLUSIONS

In summary, we explored the use of perfluoroarene-functionalized organic spacers, namely, perfluoroarene benzylammonium (F-BNA) and 1,4-phenylenedimethylammonium (F-PDMA) iodide, in 2D/3D perovskite photovoltaics. We demonstrated the formation of layered (2D) perovskite materials and their 2D/3D heterostructures by a combination of structural and optoelectronic characterization. The materials were incorporated into solar cell devices with 20% performance loss after 750 h. The performance could be further improved by adding MACl to the 3D perovskite. However, combining the 2D overlayer with MACl did not result in any additional performance gains. Furthermore, the 2D overlayers significantly enhanced operational stability compared to those without the 2D layer, maintaining high performance with only ∼15−20% degradation over 600 h, compared to ∼80% degradation without the 2D overlayer. This study highlights the potential of hybrid perfluoroarene-based perovskite materials in photovoltaics, providing a proof of concept that sets the stage for further improving device performances.

■ ASSOCIATED CONTENT

Data Availability Statement

The data presented here can be accessed at DOI: 10.5281/zenodo.1593108 (Zenodo) under the license CC-BY-4.0 (Creative Commons Attribution-ShareAlike 4.0 International).

SI Supporting Information

The Supporting Information is available free of charge at https://pubs.acs.org/doi/10.1021/acsaem.4c01710.

Materials, methods, and supporting data (PDF)

■ AUTHOR INFORMATION

Corresponding Authors

Jovana V. Milić − *Adolphe Merkle Institute/University of Fribourg, 1700 Fribourg, Switzerland;* orcid.org/0000-0002-9965-3460; Email: jovana.milic@unifr.ch

Ji-Youn Seo − *Department of Nanoenergy Engineering, Pusan National University, 46241 Busan, South Korea;* orcid.org/0000-0002-0473-1279; Email: j-y.seo@pusan.ac.kr

Authors

Weifan Luo − *Adolphe Merkle Institute/University of Fribourg, 1700 Fribourg, Switzerland*

Jong-Min Kim − *Department of Nanoenergy Engineering, Pusan National University, 46241 Busan, South Korea*

Paul Zimmermann − *Institute of Applied Physics, University of Tübingen, 72076 Tübingen, Germany*

Tim Hügli − *Adolphe Merkle Institute/University of Fribourg, 1700 Fribourg, Switzerland*

Sun-Ju Kim − *Department of Nanoenergy Engineering, Pusan National University, 46241 Busan, South Korea*

Mengqiong Zhu − *Adolphe Merkle Institute/University of Fribourg, 1700 Fribourg, Switzerland*

Ghewa AlSabeh − *Adolphe Merkle Institute/University of Fribourg, 1700 Fribourg, Switzerland; Laboratory of Photonics and Interfaces, École Polytechnique Fédérale de Lausanne, 1015 Lausanne, Switzerland*

Alexander Hinderhofer − *Institute of Applied Physics, University of Tübingen, 72076 Tübingen, Germany;* orcid.org/0000-0001-8152-6386

Frank Schreiber − *Institute of Applied Physics, University of Tübingen, 72076 Tübingen, Germany;* orcid.org/0000-0003-3659-6718

Complete contact information is available at: https://pubs.acs.org/10.1021/acsaem.4c01710

Author Contributions

$^{\perp}$W.L. and J.-M.K. contributed equally. The project was conceptualized by J.V.M. and led by W.L., who conducted the characterization of the thin films and fabrication of the solar cell devices with T.H., who synthesized the perfluoroarene precursors with M.Z. under the supervision of J.V.M. In addition, J.-M.K. measured XPS and UPS with the support of S.-J.K, under the supervision of S.-J.K., while G.A. performed TRPL characterization. P.Z. performed GIWAXS measurements and analysis under the supervision of A.H and F.S. All authors have contributed to the research and approved the manuscript.

Notes

The authors declare no competing financial interest.

■ ACKNOWLEDGMENTS

W.L., G.A., and J.V.M. acknowledge funding from the Swiss National Science Foundation (SNSF) PRIMA project no. 193174 and the fellowship from the Swiss Leading House for the Latin American Region. J.V.M. and J.-Y.S. acknowledge the Swiss Leading House for Asia (South Korea, project abbreviated as "SupraFlexi") for supporting complementary experiments. M.Z. and J.V.M. are grateful to the CSC. J.V.M. is grateful to the NCCR Bio-Inspired Materials program for support. J.-Y.S. acknowledges funding from the 2024 BK21 FOUR Program of Pusan National University. The authors are grateful to Patricia Gaina and Ethan Lim for establishing the synthetic procedures. They also thank Prof. Ullrich Steiner (Adolphe Merkle Institute) and Prof. Michael Graetzel (EPFL), colleagues at the Laboratory of Photonics and Interfaces at EPFL in Switzerland, and other international collaborators for their support. A.H. acknowledges funding from the BMBF (ERUM-Pro) project 05K19VTA. We acknowledge the ESRF for the provision of synchrotron facilities and we would like to thank Dimitry Chernyshov and Vadim Dyadkin for assistance in using beamline BM01.

■ REFERENCES

(1) Grancini, G.; Roldán-Carmona, C.; Zimmermann, I.; Mosconi, E.; Lee, X.; Martineau, D.; Narbey, S.; Oswald, F.; De Angelis, F.; Graetzel, M.; Nazeeruddin, M. K. One-Year stable perovskite solar cells by 2D/3D interface engineering. *Nat. Commun.* **2017**, *8*, 15684.

(2) Teale, S.; Degani, M.; Chen, B.; Sargent, E. H.; Grancini, G. Molecular Cation and Low-Dimensional Perovskite Surface Passivation in Perovskite Solar Cells. *Nat. Energy* **2024**, *9*, 779−792.

(3) Jena, A. K.; Kulkarni, A.; Miyasaka, T. Halide Perovskite Photovoltaics: Background, Status, and Future Prospects. *Chem. Rev.* **2019**, *119*, 3036−3103.

(4) Li, X.; Hoffman, J. M.; Kanatzidis, M. G. The 2D Halide Perovskite Rulebook: How the Spacer Influences Everything from the Structure to Optoelectronic Device Efficiency. *Chem. Rev.* **2021**, *121*, 2230−2291.

(5) Blancon, J.-C.; Even, J.; Stoumpos, C. C.; Kanatzidis, M. G.; Mohite, A. D. Semiconductor physics of organic−inorganic 2D halide perovskites. *Nat. Nanotechnol.* **2020**, *15*, 969−985.

(6) Mao, L.; Ke, W.; Pedesseau, L.; Wu, Y.; Katan, C.; Even, J.; Wasielewski, M. R.; Stoumpos, C. C.; Kanatzidis, M. G. Hybrid Dion−Jacobson 2D Lead Iodide Perovskites. *J. Am. Chem. Soc.* **2018**, *140*, 3775−3783.

(7) Zhang, F.; Park, S. Y.; Yao, C.; Lu, H.; Dunfield, S. P.; Xiao, C.; Uličná, S.; Zhao, X.; Du Hill, L.; Chen, X.; Wang, X.; Mundt, L. E.; Stone, K. H.; Schelhas, L. T.; Teeter, G.; Parkin, S.; Ratcliff, E. L.; Loo, Y.-L.; Berry, J. J.; Beard, M. C.; Yan, Y.; Larson, B. W.; Zhu, K. Metastable Dion-Jacobson 2D structure enables efficient and stable perovskite solar cells. *Science* **2022**, *375*, 71−76.

(8) Guo, W.; Yang, Z.; Dang, J.; Wang, M. Progress and perspective in Dion-Jacobson phase 2D layered perovskite optoelectronic applications. *Nano Energy* **2021**, *86*, 106129.

(9) Liu, P.; Han, N.; Wang, W.; Ran, R.; Zhou, W.; Shao, Z. High-quality Ruddlesden-Popper perovskite film formation for high-performance perovskite solar cells. *Adv. Mater.* **2021**, *33*, 2002582.

(10) Pitaro, M.; Pau, R.; Duim, H.; Mertens, M.; Van Gompel, W. T. M.; Portale, G.; Lutsen, L.; Loi, M. A. Tin-lead-metal halide perovskite solar cells with enhanced crystallinity and efficiency by addition of fluorinated long organic cation. *Appl. Phys. Rev.* **2022**, *9*, 021407.

(11) Milić, J. V. Multifunctional layered hybrid perovskites. *J. Mater. Chem. C* **2021**, *9*, 11428−11443.

(12) Mitzi, D. B.; Medeiros, D. R.; Malenfant, P. R. L. Intercalated Organic−Inorganic Perovskites Stabilized by Fluoroaryl−Aryl Interactions. *Inorg. Chem.* **2002**, *41*, 2134−2145.

(13) Milić, J. V. Perfluoroarenes: A Versatile Platform for Hybrid Perovskite Photovoltaics. *J. Phys. Chem. Lett.* **2022**, *13*, 9869−9874.

(14) Liu, Y.; Akin, S.; Pan, L.; Uchida, R.; Arora, N.; Milić, J. V.; Hinderhofer, A.; Schreiber, F.; Uhl, A. R.; Zakeeruddin, S. M.; Hagfeldt, A.; Dar, M. I.; Grätzel, M. Ultrahydrophobic 3D/2D fluoroarene bilayer-based water-resistant perovskite solar cells with efficiencies exceeding 22%. *Sci. Adv.* **2019**, *5*, No. eaaw2543.

(15) Hu, J.; Oswald, I. W.; Stuard, S. J.; Nahid, M. M.; Zhou, N.; Williams, O. F.; Guo, Z.; Yan, L.; Hu, H.; Chen, Z.; et al. Synthetic control over orientational degeneracy of spacer cations enhances solar cell efficiency in two-dimensional perovskites. *Nat. Commun.* **2019**, *10*, 1276.

(16) Almalki, M.; Dučinskas, A.; Carbone, L. C.; Pfeifer, L.; Piveteau, L.; Luo, W.; Lim, E.; Gaina, P. A.; Schouwink, P. A.; Zakeeruddin, S. M.; et al. Nanosegregation in arene-perfluoroarene π-systems for hybrid layered Dion−Jacobson perovskites. *Nanoscale* **2022**, *14*, 6771−6776.

(17) Hope, M. A.; Nakamura, T.; Ahlawat, P.; Mishra, A.; Cordova, M.; Jahanbakhshi, F.; Mladenović, M.; Runjhun, R.; Merten, L.; Hinderhofer, A.; Carlsen, B. I.; Kubicki, D. J.; Gershoni-Poranne, R.; Schneeberger, T.; Carbone, L. C.; Liu, Y.; Zakeeruddin, S. M.; Lewinski, J.; Hagfeldt, A.; Schreiber, F.; Rothlisberger, U.; Grätzel, M.; Milić, J. V.; Emsley, L. Nanoscale Phase Segregation in Supramolecular π-Templating for Hybrid Perovskite Photovoltaics from NMR Crystallography. *J. Am. Chem. Soc.* **2021**, *143*, 1529−1538.

(18) Li, Y.; Milić, J. V.; Ummadisingu, A.; Seo, J.-Y.; Im, J.-H.; Kim, H.-S.; Liu, Y.; Dar, M. I.; Zakeeruddin, S. M.; Wang, P.; Hagfeldt, A.; Grätzel, M. Bifunctional Organic Spacers for Formamidinium-Based Hybrid Dion−Jacobson Two-Dimensional Perovskite Solar Cells. *Nano Lett.* **2019**, *19*, 150−157.

(19) Loizos, M.; Rogdakis, K.; Luo, W.; Zimmermann, P.; Hinderhofer, A.; Lukic, J.; Tountas, M.; Schreiber, F.; Milic, J. V.; Kymakis, E. Resistive Switching Memories with Enhanced Durability Enabled by Mixed-Dimensional Perfluoroarene Perovskite Heterostructures. *Nanoscale Horiz.* **2024**, *9*, 1146−1154.

(20) Zhao, W.; Wu, M.; Liu, Z.; Yang, S.; Li, Y.; Wang, J.; Yang, L.; Han, Y.; Liu, S.; Frank. Orientation Engineering via 2D Seeding for Stable 24.83% Efficiency Perovskite Solar Cells. *Adv. Energy Mater.* **2023**, *13*, 2204260.

(21) Li, P.; Zhang, Y.; Liang, C.; Xing, G.; Liu, X.; Li, F.; Liu, X.; Hu, X.; Shao, G.; Song, Y. Phase Pure 2D Perovskite for High-Performance 2D−3D Heterostructured Perovskite Solar Cells. *Adv. Mater.* **2018**, *30*, 1805323.

(22) Tan, W. L.; McNeill, C. R. X-ray diffraction of photovoltaic perovskites: Principles and applications. *Appl. Phys. Rev.* **2022**, *9*, 021310.

(23) Alanazi, A. Q.; Almalki, M. H.; Mishra, A.; Kubicki, D. J.; Wang, Z.; Merten, L.; Eickemeyer, F. T.; Zhang, H.; Ren, D.; Alyamani, A. Y.; Albrithen, H.; Albadri, A.; Alotaibi, M. H.; Hinderhofer, A.; Zakeeruddin, S. M.; Schreiber, F.; Hagfeldt, A.; Emsley, L.; Milić, J. V.; Graetzel, M. Benzylammonium-Mediated Formamidinium Lead Iodide Perovskite Phase Stabilization for Photovoltaics. *Adv. Funct. Mater.* **2021**, *31*, 2101163.

(24) Chen, P.; Bai, Y.; Wang, S.; Lyu, M.; Yun, J.-H.; Wang, L. In Situ Growth of 2D Perovskite Capping Layer for Stable and Efficient Perovskite Solar Cells. *Adv. Funct. Mater.* **2018**, *28*, 1706923.

(25) Zouhair, S.; Yoo, S. M.; Bogachuk, D.; Herterich, J. P.; Lim, J.; Kanda, H.; Son, B.; Yun, H. J.; Würfel, U.; Chahboun, A.; et al. Employing 2D-perovskite as an electron blocking layer in highly efficient (18.5%) perovskite solar cells with printable low temperature carbon electrode. *Adv. Energy Mater.* **2022**, *12*, 2200837.

(26) Luo, L.; Zeng, H.; Wang, Z.; Li, M.; You, S.; Chen, B.; Maxwell, A.; An, Q.; Cui, L.; Luo, D.; et al. Stabilization of 3D/2D perovskite heterostructures via inhibition of ion diffusion by cross-linked polymers for solar cells with improved performance. *Nat. Energy* **2023**, *8*, 294−303.

(27) Stolterfoht, M.; Wolff, C. M.; Márquez, J. A.; Zhang, S.; Hages, C. J.; Rothhardt, D.; Albrecht, S.; Burn, P. L.; Meredith, P.; Unold, T.; et al. Visualization and suppression of interfacial recombination for high-efficiency large-area pin perovskite solar cells. *Nat. Energy* **2018**, *3*, 847−854.

(28) Chen, A. Z.; Foley, B. J.; Ma, J. H.; Alpert, M. R.; Niezgoda, J. S.; Choi, J. J. Crystallographic orientation propagation in metal halide perovskite thin films. *J. Mater. Chem. A* **2017**, *5*, 7796−7800.

(29) Deng, L.; Yang, H.; Liu, Z.; Yang, X.; Huang, Z.; Yu, H.; Wang, K.; Li, J. Effective Phase Control for High-Performance Red-Light-Emitting Quasi-2D Perovskite Solar Cells via MACl Additive. *ACS Appl. Energy Mater.* **2021**, *4*, 2856−2863.

(30) Ma, Q.; Zhang, Y.; Lu, C.; Zhang, R.; Wang, X.; Zhang, W.; Jiang, Z. MACl-Induced Controlled Crystallization in Sequentially Deposited Perovskites for High-Efficiency and Stable Perovskite Solar Cells. *Coatings* **2023**, *13*, 1885.

(31) Boyd, C. C.; Cheacharoen, R.; Leijtens, T.; McGehee, M. D. Understanding degradation mechanisms and improving stability of perovskite photovoltaics. *Chem. Rev.* **2018**, *119*, 3418−3451.